The mechanisms of alteration of a homogeneous U0.73Pu0.27O2 MOx fuel under alpha radiolysis of water

Valentin Kerleguer, Christophe Jegou, Laurent de Windt, Véronique Broudic, Gauthier Jouan, Sandrine Miro, Florent Tocino, Christelle Martin

Version of Record: https://www.sciencedirect.com/science/article/pii/S0022311519307755
Manuscript_60ef660b7d619c36431b4b7d2bcec389

The mechanisms of alteration of a homogeneous $U_{0.73}Pu_{0.27}O_2$ MOx Fuel under alpha radiolysis of water

Valentin Kerleguer[a,b], Christophe Jégou[a], Laurent De Windt[b], Véronique Broudic[a], Gauthier Jouan[c], Sandrine Miro[a], Florent Tocino[d], Christelle Martin[e]

[a]*Commissariat à l'Energie Atomique et aux Energies Alternatives (CEA), Centre de Marcoule, DEN,MAR,DE2D,SEVT,LMPA, Bat. 166, BP 17171, 30207, Bagnols-sur-Cèze cedex, France*

[b]*MINES ParisTech, PSL University, Centre de Géosciences, 35 rue Saint Honoré, 77305 Fontainebleau*

[c]*Commissariat à l'Energie Atomique et aux Energies Alternatives (CEA), Centre de Marcoule, DEN,DMRC,SFMA,LCC, Bat. 166, BP 17171, 30207, Bagnols-sur-Cèze cedex, France*

[d]*Electricité de France (EDF), Les Renardières Research Center, Route de Sens Ecuelles, 77250 Moret-sur-Loing, France*

[e]*Agence Nationale pour la gestion des Déchets Radioactifs (ANDRA), 1/7 rue Jean Monnet, 92298 Châtenay-Malabry Cedex, France*

ABSTRACT

An homogeneous MOx fuel with 24 wt.% of plutonium was leached in a carbonated water (10^{-2} M) under argon ($[O_2] < 1$ vppm) for one year in order to assess the leaching behaviour of U-Pu oxide solid solutions and more specifically to simulate the behaviour of Pu enriched agglomerates characteristic of heterogeneous Mimas MOx fuel. The alpha activity of the pellets was 2.2×10^9 Bq.g^{-1}. Two successive dissolution regimes were observed: an initial dissolution with a uranium release rate of 1.2×10^{-4} mol$_U$.m^{-2}.d^{-1}, and then, a long-term dissolution regime with a rate of 7.6×10^{-6} mol$_U$.m^{-2}.d^{-1}. The H_2O_2 concentration was under the detection limit of 1×10^{-7} mol.L^{-1}. Pu concentration in the homogeneous solution was constant around 10^{-9} mol.L^{-1} throughout the duration of the experiment, in accordance with a thermodynamic equilibrium controlled by an amorphous $Pu(OH)_4$ phase. SEM – WDS analysis confirmed a Pu-enriched layer at the surface of the pellets with Pu contents up to 39 wt.%. This Pu-enriched layer becomes more resistant against leaching than the pristine surface. Despite this Pu enrichment, H_2O_2 concentration remained very low in the homogeneous solution. Different mechanisms of consumption can be considered, such as the oxidative dissolution of the pellet, the precipitation of U or Pu peroxides or the catalytic disproportionation. As the precipitation of peroxides at the surface was discarded by Raman spectroscopy and the oxidative dissolution was very limited, the low H_2O_2 concentration was likely due to a higher catalytic disproportionation of H_2O_2 by the Pu-enriched layer. Mass balance calculation showed that H_2O_2 disproportionation represented 99 % of the H_2O_2 consumption for the homogeneous MOx, against 86 % for UO_2 pellets. These results shed new light on the Pu stabilizing mechanisms against the oxidative dissolution that can be applied to model the behaviour of different MOx fuels under long-term disposal conditions.

Keywords. Hydrogen peroxide, leaching, radiolysis, radioactive waste, plutonium, MOx fuel.

1. INTRODUCTION

In the hypothesis of direct disposal of spent fuel in a deep geological repository, interactions between the fuel mainly composed of UO_2 and its environment must be understood. The dissolution rate of the spent fuel matrix, which depends on the redox conditions on the fuel surface, will have a major impact on the release of radionuclides into the environment. In the anoxic and reductive environment found in the deep geological conditions, the release rate is very low as well as the uranium concentrations (around 10^{-9} mol.L^{-1}). A thermodynamic control of the alteration by UO_2:$2H_2O$(am) [1] is classically considered without any change in the oxidation state of uranium. However, when assessing the long-term behavior of spent nuclear fuels (irradiated MOx fuels or irradiated UO_2 fuels), one needs to consider both alpha irradiation (predominant on the long term) and beta/gamma irradiation of long-lived actinides, activation and fission products. Emission of strong alpha and beta/gamma radiation from spent nuclear fuels to adjacent groundwater causes a radiolytical decomposition of the aqueous solution. Radiolysis of water in the near field is accompanied by the formation of equimolar amounts of oxidizing and reducing species. Due to the relatively high reactivity of oxidizing radiolysis products, in particular H_2O_2, compared to the reactivity of the main reducing radiolysis product H_2, essentially an oxidative environment is expected to result from the radiolysis in the close vicinity of spent nuclear fuels [2]. Uranium can therefore be oxidized and form more soluble species leading to the dissolution of the fuel and, ultimately, to the precipitation of uranium secondary phases [3]. This sequence of mechanisms is known as the radiolytic dissolution of UO_2.

In carbonated water, strong uranyl carbonate complexes prevent the precipitation of secondary species and uranium can be used as a tracer of the alteration [4,5]. The dissolution rate of U(VI) from the UO_2 surface is also enhanced by such carbonate complexes [6]. Therefore, the radiolytic dissolution mechanism is mostly controlled by the oxidation of UO_2 by H_2O_2 and the uranium concentration can be used to determine the intrinsic kinetic rate constant of UO_2 oxidation/dissolution. This kinetic has already been extensively studied for simple UO_2 matrix, but there is still a lack of information about the behaviour of MOx ($U_{1-x}Pu_xO_2$) fuels. The Pu content and microstructure are the two key parameters to be considered to extend the knowledge from UO_2 to MOx matrices. Moreover, it is worth noting that water radiolysis is a major difference between unirradiated UOx and MOx fuels. The Am/Pu-content of MOx corresponds to an inherent radiolytic activity in the aqueous solution in contact with the fuel pellets.

The French MOx fuel, manufactured with the MIMAS process (MIcronization of a MASter blend), is highly heterogeneous and its microstructure can be characterized according to three poles: the UO_2 matrix with up to 2.7 wt.% of plutonium, the Pu-enriched agglomerates with up to 20.2 wt.% of plutonium, and an intermediate phase with up to 7 wt.% of Pu [7,8]. The surface covered by the Pu-agglomerates represents approximately 10 %, while the other two phases represented roughly 45 % each one. Odorowski et al. [8,9] studied the leaching behaviour in carbonated water of this unirradiated heterogeneous MOx. Their results indicated a very fast dissolution of the UO_2 grains, likely due to the high alpha-activity induced by the surrounding plutonium agglomerates. On the contrary, the plutonium agglomerates were not altered over the leaching experiment. This is consistent

with the stabilizing effect of the plutonium on the oxidation of the fluorite matrix [8,9]. Similar alteration experiments with heterogeneous MOx of higher Pu content (24%) were conducted by Bauhn et al [10] in carbonated water with Ar or H_2 atmospheres. The authors also concluded that Pu led to a higher stability of the fluorite structure against oxidation and therefore against dissolution.

To the best of our knowledge, no data are available in the literature on the kinetics of dissolution of homogeneous solid solution with high plutonium content close to those of plutonium enriched aggregate (>20 wt.%) under environmental conditions. This is a key point required for the safety assessment of eventual future disposal of any kind of MOx fuels. More generally, data is also needed for a better understanding of Pu-U oxide solid solutions chemistry in water. For these purposes, a fresh homogeneous MOx (i.e. before irradiation in a nuclear reactor) with 24 wt.% of Pu was leached in carbonated water under anoxic conditions over one year in order to simulate the behaviour of the Pu-rich agglomerates of MIMAS MOx fuels and to get kinetic data to model the radiolytic dissolution. The uranium, plutonium and hydrogen peroxide concentrations were measured over time, as well as the Eh and pH parameters. The mass balance between aqueous, colloidal and precipitated/sorbed fractions was quantitatively determined at the end of the experiment. Surface characterization, involving SEM-WDS and Raman spectroscopy, was achieved on the homogeneous MOx pellets before and after leaching. Solubility diagrams were calculated with CHESS software and the ThermoChimie database to support the data discussion.

2. MATERIALS AND METHODS

2.1 MATERIALS

The homogeneous MOx pellets were manufactured in 1985 with the co-milling Cadarache process (COCA process). The metal stoichiometry in the oxide was $U_{0.73}Pu_{0.27}$ with an exact oxygen–to-metal ratio (O/M) = 1.983 and a density of 10.421 $g.cm^{-3}$. The polished pellets (around 1 mm thickness and 5.4 mm diameter) were annealed at 1100°C for 5 hours in an Ar/H_2 4% atmosphere before the experiments in order to restore the stoichiometry (O/M = 2.00) and a surface state free of potentially hydrated phases formed during the storage of the pellets. The size and specific surface (without roughness factor) of the cylindrical pellets are given in Table 1. The uncertainties were estimated following the Eurachem guide for analytical uncertainties [11].

The isotopic composition at the beginning of the leaching experiment was derived from isotopic decay calculations considering the JEFF2.2 database (Table 2) with an uncertainty of 0.1%. The α, β and γ heat powers related to this isotopic composition were 1.94×10^{-3}, 1.54×10^{-5} and 5.08×10^{-6} W/g_{MOX}, respectively. The α-activity of a pellet was 2.2×10^{9} $Bq.g^{-1}_{MOx}$, which corresponds to an α-dose rate received by the solution of 9730 $Gy.h^{-1}$ based on the Sunder calculation method [12]. The β and γ dose rates were calculated at different distances from the pellet surface using the Vaskin© 3.1.0 and the Mercurad© 1.04 codes respectively. The β dose rate was 0.52 $mGy.h^{-1}$ at 100 µm from the surface and mainly due to traces of ^{234m}Pa. This dose rate was too low and therefore not considered. The γ dose rate, mainly produced by the ^{241}Am, quickly dropped, i.e. 110 $mGy.h^{-1}$ at 100

µm, 4 mGy.h^{-1} at 1 cm, and only 0.2 mGy.h^{-1} at 5 cm from the surface. The α dose rate is therefore 5 to 6 orders of magnitude higher than the β/γ dose rates.

An average range of 40 µm was considered for α-particles, leading to an irradiated volume of 4.10^{-3} cm^3, while the whole volume was considered for γ radiations, i.e. 150 cm^3. Considering these irradiated volumes with their respective dose rates, the deposited α energy into the solution remains two orders of magnitude higher than the β/γ energies. Therefore, α irradiation is assumed to be the main source of H_2O_2 production.

To finish, it is important to remember that this is a model material that has advantages and limitations with respect to the spent nuclear fuel. This model material has a major alpha activity that will be well predominant for the spent fuel under geological disposal conditions. Although this alpha activity is high it allows to specifically study the oxidative dissolution under alpha radiolysis of the fluorite structure. Regarding the chemistry evolution after irradiation inside the reactor, the plutonium content will also decrease and that of this model material remains quite high. The average weight content of plutonium in the Pu-enriched agglomerates can drop to 10% with significant local fluctuations after irradiation. Indeed local plutonium contents of the order of 20% can be observed in the center of the Pu-enriched agglomerates after irradiation. Irradiation will also induce the generation of fission products that can limit oxidation [13,14] and change the microstructure of the fuel [15]. It is therefore by combining studies on model materials and irradiated fuel that the mechanisms of dissolution can be understood.

2.2 LEACHING EXPERIMENT

After annealing, pellets were transferred to an anoxic alpha-glovebox (argon atmosphere, [O_2] < 2 vppm) for the leaching experiment. The two MOx pellets were submitted to 10 pre-leaching cycles in carbonated water ([$NaHCO_3$] = 10^{-3} mol.L^{-1}) in order to remove the potential oxidized layer that could have been formed on the surface. The two pellets were then inserted in a titanium dioxide sample holder and leached in 155 mL of carbonated water ([$NaHCO_3$] = 10^{-2} mol.L^{-1}). All the parts of the leaching reactor in direct contact with solution were in titanium dioxide, which is relatively chemically inert towards radiolytical species. The leaching test lasted 342 days, and 9 solution samples were taken at 1, 8, 15, 30, 78, 90, 155, 251 and 342 days. The last sample was filtered at 0.45 µm (VWR cellulose acetate filter) and ultra-filtered at 20 nm (Whatman Anodisc inorganic filter) to determine the presence of any colloids. At the end of the experiment, pellets were dried (residual water absorption on a propylene wiper) and stored under argon atmosphere until surface characterization. The remaining volume of solution was collected and acidified at 1 mol.L^{-1} with nitric acid HNO_3. Then, the reactor was rinsed three times with 155 mL of ultrapure nitric acid (HNO_3). The first rinsing was done with a 2M nitric acid solution and the last two rinsings with a 1M solution. The duration of each rinsing was 24 hours. Finally, three successive rinses with 180 mL ultra-pure water were performed. Solution samples were taken and analysed for each acidification and rinse. These acid rinses permitted the total quantification of colloids and species sorbed or precipitated on the walls of the titanium oxide reactor.

2.3 SOLUTION ANALYSIS

The uranium concentration was determined by laser-induced kinetic phosphorescence with the Chemchek KPA11 Kinetic Phosphorescence Analyser, with a quantification limit of 0.1 µg.L^{-1}. H_2O_2 concentration was measured by chemiluminescence with the Turner BioSystems luminometer (TD 20/20) using the standard addition method for concentrations ranging from 1×10^{-7} to 1×10^{-5} mol.L^{-1}. The plutonium concentration was measured by alpha-spectrometry with the Canberra Alpha Analyst spectrometer and by alpha-counting with the Eurisys IN 20 alpha-beta multi-detector counter. Eh and pH were regularly measured ex-situ during the leaching experiment and in-situ at the end of the test by using the WTW SenTix ORP electrode (for Eh) and the Mettler Toledo LoT406-M6-DXK-S7/25 electrode (for pH).

2.4 SURFACE CHARACTERIZATION

The initial state of the pellet surface was characterized by Scanning Electron Microscopy (SEM) with a JEOL JSM 6300 microscope. The electron probe micro-analyser (EPMA) technique was used to determine the distributions of Pu in the sample with a spatial resolution of 1 µm^3. CAMECA SX 50 EPMA (EPMA Cameca) equipped with four X-ray spectrometers and thallium acid pthalate/polyethylene terephthalate crystals was operated under an acceleration voltage of 20 kV and 20-nA stabilized beam. To quantify the Pu content, the instrument was calibrated with plutonium-bearing glasses (1.74 wt% Pu).

After leaching, one of the pellets was observed by SEM with a ZEISS SUPRA 55. This apparatus is equipped with modified EDS X-act and WDS Oxford Instrument detectors. An accelerating voltage between 5 and 20 kV with a current of 39 nA was applied for imaging, and a voltage of 20 kV with a current of 39 nA for WDS analyses. Technical details on the system can be found elsewhere [16]. The estimated depth of the analysis for this material is 600 nm, and the standard used to calibrate the WDS was a 25 wt.% Pu homogeneous MOx. Band Mα and Mβ were used for uranium and plutonium, respectively.

Raman spectra were acquired with a HORIBA LabRam-HR800 Raman spectrometer coupled with a nuclearized microscope (Optique Peter) in a hot cell. An yttrium aluminium garnet laser (532 nm) with adjustable output powers was used as excitation source. The laser was focused through a x100 objective to a spot size of around 1 µm^2 with an incident laser power weaker than 1 mW. Technical details on the system can be found in the paper of Jégou et al. [9]. Approximately 40 Raman spectra were acquired after leaching with five runs and an exposure duration of 180 s per run.

2.5 SOLUBILITY DIAGRAMS AND MODELLING

The CHESS software [17] and the ThermoChimie thermodynamic database [18] were used to calculate the solubility diagrams of U and Pu applicable to the long-term leaching of the MOx pellet. UO_2 (crystallized), β-$UO_2(OH)_2$, and PuO_2 (crystallized) have been discarded, as they are not expected to precipitate in such conditions. The MOx dissolution was modelled using kinetic reactions, which will be described later in the article.

3. RESULTS AND DISCUSSION

3.1 INITIAL STATE OF THE PELLETS

After annealing, the plutonium distribution was assessed using EPMA and Raman Spectroscopy. Two EPMA linear profiles with 35 µm steps confirmed a constant Pu content at 24 ± 0.5 wt.% over 260 points (2x130 steps of 35 µm) as presented in Fig.1. The weight percentages in oxide are fully consistent with the stoichiometry $(U_{0.73}Pu_{0.27})O_2$. Some fluctuations of the U and Pu contents are observed on some analysis points. These fluctuations do not exceed 10% in general and only two or three analyses with slightly lower contents were observed (13 to 17% by weight of Pu).

The Raman spectra (see Fig. 8 in Sec. 3.3.2) showed a T_{2g} band position at 455 cm^{-1} in perfect agreement with the chemical composition of the solid solution $U_{0.73}Pu_{0.27}O_2$ studied. The position of this band, associated to the vibration of the actinide-oxygen bond, shifts towards the high wavenumbers with the plutonium content as demonstrated by Elorrieta et al. [19]. The position is in line with the data of Elorrieta and confirms the homogeneous nature of the solid solution at the micron scale as already revealed by EPMA. Moreover, no traces of oxidized phases were observed by Raman spectroscopy. The intense 2LO band (around 1160 cm^{-1}) and the absence of a signal around 630 cm^{-1} indicate the absence of M_4O_9 type phase.

After the surface characterization, which confirmed the homogeneity of the pellets, the pellets were submitted to 10 pre-leaching cycles in carbonated water (see section 2.2). Fig. 2 shows that the uranium concentration was under 10 $\mu g.L^{-1}$ and no initial release peak was observed which demonstrates the absence of an oxidized layer [20].

3.2 SOLUTION ANALYSIS AND GLOBAL DISSOLUTION RATE

The pH of the solution was slightly alkaline and constantly buffered to 9.3±0.2 by the hydrogenocarbonate (HCO_3^-) ions. The redox potential was around 0.350±0.1 V/SHE, which corresponds to mildly oxidizing conditions at this pH.

Fig. 3 shows the evolution over time of the uranium concentrations. Two successive dissolution regimes are observed: first, an initial dissolution with a uranium release rate r_u of 1.20×10^{-4} ± 0.12×10^{-4} $mol_U.m^{-2}.d^{-1}$ (28.6 ± 2.8 $mg_U.m^{-2}.d^{-1}$) over the first 30 days, and then, a long-term dissolution regime with a mean rate r_u of 7.6×10^{-6} ± 0.8×10^{-6} $mol_U.m^{-2}.d^{-1}$ (1.8 ± 0.19 $mg_U.m^{-2}.d^{-1}$) between 78 and 342 days. The alteration rates of the oxide (MOx) are respectively 44 and 2.8 $mg_{MOx}.m^{-2}.d^{-1}$, considering the stoichiometry $U_{0.73}Pu_{0.27}O_2$. The initial rate is not due to the leaching of any pre-oxidized layer, as discussed in Sec. 3.1. In the present experiment, the long-term rate is not related to any precipitation of uranium secondary phases or strong sorption as indicated by the speciation diagram of Fig. 5a. Indeed, the soluble fraction of the total uranium release (190 ± 10 µg) is dominant (> 95 wt.%) (Fig. 4). The colloidal fraction is low (<1 wt.%) and almost no U is precipitated or sorbed (around 4 wt.%) onto the TiO_2 surface. It is consistent with the uranium solubility diagram of Fig. 5, where uranium is stabilized in solution as the strong U(VI) complex $UO_2(CO_3)_3^{4-}$, in the range 10^{-6} – 10^{-4} $mol.L^{-1}$ (at pH 9 and Eh around 0.35 – 0.40 V), well below the schoepite solubility limit.

The H_2O_2 concentration over the duration of the leaching experiment was under the limit of detection (around 1-2×10^{-7} mol.L^{-1}).

The plutonium concentration in solution is almost constant, around 10^{-9} mol.L^{-1} (Fig. 3) over the duration of the leaching test. The solubility diagram of plutonium (Fig. 5) shows that the predominant species in solution is the carbonate complex $Pu(CO_3)_2(OH)_2^{2-}$ at pH 9 and Eh around 0.35 – 0.40 V. Under such chemical conditions, the plutonium concentration is compatible with a thermodynamic control by the amorphous phase $Pu(OH)_4$ [21]. The amorphous phase PuO_2:$2H_2O$ [22] has the same stoichiometry as $Pu(OH)_4$(am), but clearly it does not match with the present experimental data. However, the system could be in a metastable condition with respect to this phase. Eventually, the hydrated colloidal phase PuO_2 equilibrium is not far from the experimental data, but slightly too soluble. Contrary to the uranium, the soluble plutonium fraction (2 wt.%) was negligible, few colloids were detected (<1 wt% with a cut-off at 20 nm). The majority of the released plutonium was precipitated (or maybe partially sorbed) on the walls of the reactor (97 wt.%) (Fig. 4). The total plutonium release was 1.2 ± 1.0 µg, which is much lower than the 70 µg calculated considering a congruent dissolution with the uranium.

3.3 SURFACE CHARACTERIZATION AFTER LEACHING

3.3.1 Quantitative SEM-WDS analysis

After leaching, one of the pellets was analysed by SEM-WDS. Fig. 6 show SEM images of homogeneous MOx after one year of leaching in carbonated water (10^{-2} mol.L^{-1}). Globally, there is a microstructural homogeneity of the surface and no particular dissolution pattern was observed over the pellet surface. Only scarce occurrence of dissolution pits was observed. On the contrary, the surface of a heterogeneous MIMAS MOx pellet leached under the same experimental conditions [7] was significantly altered with a high occurrence of dissolution pits corresponding to former UO_2-rich grains as indicated by the SEM-WDS analysis (Fig. 7). Otherwise, the SEM images did not show any secondary phase precipitation for both types of MOx.

The quantitative U and Pu analyses indicated a Pu enrichment of the surface, with a homogeneous Pu content (Pu/(U+Pu)) of 39 wt.% (against 27 wt.%, initially) (Table 3). This enrichment is likely due to the missing Pu fraction (70 µg). Such a behaviour was already observed by Stroes-Gascoyne et al. [5] on UO_2 pellets doped with 0.6 Pu wt.%. They concluded that the uranium release was very fast compared to the plutonium one, leading to a Pu enrichment of the pellet surface.

3.3.2 Raman spectroscopy

The observed Pu-enrichment can have different origins, such as a uranium depletion of the fluorite structure, the precipitation of secondary phases like peroxides or either the formation of an amorphous $Pu(OH)_4$ layer as suggested by the solubility diagram of plutonium (Fig. 5). Raman spectroscopy was used in order to bring elements of understanding. The laser beam power was lower for the analysis of the altered sample (<1 mW) than for the pristine one (2.8 mW) to avoid disturbing

the surface by oxidation or dehydration. This explains the higher background noise of the former spectra in Fig. 8. The spectra obtained before and after leaching were basically the same despite the Pu enrichment of the surface observed through WDS analysis. They can be interpreted as follows:

- In the case of a uranium depletion of the fluorite structure, the T_{2g} band was expected to shift from 455 cm^{-1} (for the initial solid solution $U_{0.73}Pu_{0.27}O_2$) to higher wavenumbers considering a strengthening of the Pu-O bound. For a hypothetic $U_{0.61}Pu_{0.39}O_2$ (as analysed by SEM-WDS), the wavenumber should have increased to approximately 460 cm^{-1} [19]. No significant shift is observed experimentally.
- In the case of a uranium or plutonium peroxide precipitation, a peak would be visible between 840 and 870 cm^{-1}, typical of O-O peroxide bond in plutonium peroxocarbonate [23] or uranium peroxides like studtite or metastudtite [24,25]. The peroxide bond does not appear on the Raman spectra.
- Uranyl bonds between 820 and 840 cm^{-1} are not observed indicating the absence of secondary phases such as schoepite and confirming the complexing effect of carbonates.
- To the best of our knowledge, no Raman spectra of $Pu(OH)_4(am)$ are available in the literature. The OH groups have a signature at high energies but unfortunately the acquisition range was restricted to 1400 cm^{-1}. Without presuming the formation process of the plutonium hydroxide on the surface of the pellets (precipitation from the solution or local plutonium hydrolysis and recondensation on the surface), some structural data are available on the colloids and hydroxides of plutonium IV in the literature [26]. Anyway, no evolution of the Raman signal has been observed in our study, which may disclose the formation of an amorphous compound. This does not allow dismissing the hypothesis of its formation. Indeed, it may not have a Raman signature or its thickness could be too small in relation to the spatial resolution of our Raman spectrometer (about 1 μm^3 [27]). Thickness would not exceed 150 nm assuming that the plutonium enrichment observed is entirely due to the formation of such a $Pu(OH)_4(am)$ film with a density between 5 and 6 $g.cm^{-3}$.

3.4 INFLUENCE OF THE PU CONTENT AND MICROSTRUCTURE

3.4.1 Long-term catalytic disproportionation of H_2O_2 on MOx

It is reasonable to assume that hydrogen peroxide is the main contributor to the oxidative dissolution of the MOx matrix [28,29]. The H_2O_2 concentration in solution is controlled by one production term due to water radiolysis and two consumption terms related to disproportionation and MOx oxidation. In addition, a blank experiment on H_2O_2 disproportionation in pure water inside a similar TiO_2 reactor had shown that this process was very slow (< 1% per day). Therefore, the overall rate of H_2O_2 concentration evolution (due to both formation and consumption) can be quantitatively estimated by the following equation assuming a first order law on the dissolved H_2O_2 for the disproportionation [30] as well as for the oxidation:

$$\frac{d[H_2O_2(aq)]}{dt} = \left(k^{prod} - k^{disprop}\,[H_2O_2(aq)] - k_U^{oxid}\,[H_2O_2(aq)]\right) A_v \qquad (1)$$

where A_v = 8x10^{-4} m^2.L^{-1} is the volumetric surface of the MOx pellet. For the sake of the discussion, the H_2O_2 was considered constant at the limit of quantification (LQ) of 1x10^{-7} mol.L^{-1}, i.e. the potentially most oxidizing conditions, and therefore:

$$\frac{d[H_2O_2(aq)]}{dt} = 0 \quad (2)$$

The combination of Eqs (1) and (2) leads to:

$$k^{prod} A_v = k^{disprop} [H_2O_2(aq)] A_v + k_U^{oxid} [H_2O_2(aq)] A_v \quad (3)$$

As explained in Sec. 2.1, the β/γ dose rate was not considered. The alpha dose rate was calculated to be 9730 Gy.h^{-1} using the Sunder's method [12] and an alpha primary yield of 0.98 molecule/100eV was considered for hydrogen peroxide production. The corresponding H_2O_2 production rate is 1.10x10^{-8} mol.m^{-2}.s^{-1} (i.e. 9.5x10^{-4} mol.m^{-2}.d^{-1}) assuming an average α-particle range of 40 µm in water and the geometric surface of the pellets (Table 1). With such a production rate, the concentration of H_2O_2 would increase by 8x10^{-7} mol.L^{-1}.d^{-1}, and thus be above the limit of quantification already in the very first hours, if there was no consumption by disproportionation and uranium oxidation.

In carbonated water, the dissolution of uranium VI phases is often considered as instantaneous; the uranium oxidation of the MOx surface by hydrogen peroxide is therefore directly linked to the uranium release rate. The experimental dissolution rates of Sec. 3.2 can be used to determine the H_2O_2 consumption rate by the uranium oxidation in the MOx. Furthermore, one mole of uranyl in solution corresponds to one mole of H_2O_2 consumption, thus the rate of uranium dissolution is equal to the rate of H_2O_2 consumption.

For the initial dissolution, the uranium oxidation rate (k_U^{oxid}×[H_2O_2(aq)]) was estimated at 1.4x10^{-9} mol.m^{-2}.s^{-1} (i.e. 1.2x10^{-4} mol.m^{-2}.d^{-1}). This indicates that 12.5% of the radiolytically-produced H_2O_2 was consumed by oxidation of the MOx pellet during the initial dissolution step. Considering the calculated H_2O_2 production rate, the H_2O_2 concentration after 30 days should be two order of magnitude higher that the detection limit, but was not observed in the experiment. Therefore, the remaining 87.5% of radiolytically-produced H_2O_2 were consumed elsewhere and in particular by disproportionation. This is consistent with the disproportionation estimated on UO_2 pellets [31,32]. Considering the catalytic disproportionation of H_2O_2 as the main mechanism, a disproportionation rate (k^{disp}×[H_2O_2(aq)]) of 9.6x10^{-9} mol.m^{-2}.s^{-1} was estimated, and hence a rate constant k^{disp} of 9.6x10^{-2} L.m^{-2}.s^{-1} could be calculated.

The long-term dissolution rate (k_U^{oxid}×[H_2O_2(aq)]) was estimated as 8.8x10^{-11} mol.m^{-2}.s^{-1} (i.e. 7.6x10^{-6} mol.m^{-2}.d^{-1}), indicating that less than 1% of the H_2O_2 was consumed by the oxidation of the MOx pellet during the long-term dissolution. The H_2O_2 concentration was under the limit of quantification, meaning that 99% of the radiolytically-produced H_2O_2 was consumed by the catalytic disproportionation on the MOx pellet surface. Such a high consumption is consistent with the values that have been experimentally determined for Pu-doped UO_2 and SIMFUEL pellets [31,32]. Considering the catalytic disproportionation of H_2O_2 as the main mechanism, a disproportionation rate (k^{disp}×[H_2O_2(aq)]) of 1.1x10^{-8} mol.m^{-2}.s^{-1} was estimated, and hence a rate constant k^{disp} of 1.1x10^{-1} L.m^{-2}.s^{-1} could be calculated.

The evolution of the catalytic properties (k^{disp}) of the MOx surface can be induced by the Pu enrichment. Different disproportionation mechanisms involving different oxidation state of plutonium can be considered. Korzhavyi et al. described a possible surface-catalysed decomposition of H_2O_2 on the PuO_2 surface by the mean of the reactions 4 and 5 [33]:

$$4\ PuO_2 + H_2O_2 \rightarrow Pu_4O_9 + H_2O \quad (4)$$

$$Pu_4O_9 + H_2O_2 \rightarrow 4\ PuO_2 + H_2O + O_2 \quad (5)$$

Similar mechanisms were already described in the literature for uranium [34,35], however this mechanism is not likely to occur as no evidence of plutonium oxidation was actually confirmed in the solid. Another possible mechanism could be the reduction of Pu(IV) to Pu(III), followed by the oxidation of the latter [36]:

$$2\ Pu^{4+} + H_2O_2 \rightarrow 2\ Pu^{3+} + O_2 + 2\ H^+ \quad (6)$$

$$2\ Pu^{3+} + H_2O_2 + 2\ H^+ \rightarrow 2\ Pu^{4+} + 2\ H_2O \quad (7)$$

In the absence of data on plutonium speciation at the surface it is difficult to conclude, nevertheless these processes cannot be discarded at this stage.

Finally, it is worth noticing that the Pu-enrichment of the surface could have led to an α-dose rate increase at the solid/water interface, which could increase the H_2O_2 production term. Stroes-Gascoyne et al. [5] observed a similar Pu enrichment and considered that the alpha dose rate is likely to stay relatively constant as the altered layer of the pellets (0.1 - 0.4 µm) was much smaller than the average alpha particles range in the matrix (~12 µm). Indeed, the alpha emitters located at several microns in the pellet are the main contributor to the energy deposit at the extreme surface through the Bragg peak.

3.4.2 Effect of the Pu-enriched layer, passivation versus enhanced disproportionation

Considering a constant H_2O_2 concentration of $1x10^{-7}$ mol.L^{-1} (i.e. the limit of quantification), two kinetic rate constants for the uranium dissolution (k_U^{oxid}) may be calculated from the experimental uranium data: an initial kinetic rate constant of $1.4x10^{-2}$ L.m^{-2}.s^{-1} and a long term kinetic rate constant of $8.8x10^{-4}$ L.m^{-2}.s^{-1} (approximately 16 times lower).

Since the kinetics are determined following the uranium release, the decrease in the rate constant could be due to the depletion in uranium of the altered layer. On the other hand, the decrease is probably linked to the formation of a Pu-enriched layer at the surface of the pellets. It has been demonstrated in the literature that high Pu contents have a stabilizing effect on the fluorite oxide matrix and decrease its reactivity towards oxidation [7,9,14]. However, in this case, the formation of the amorphous $Pu(OH)_4$ layer has probably a stabilizing role and a H_2O_2 disproportion role. The deposition of amorphous hydroxide layers such as $Pu(OH)_4$ is quite consistent with the observation made on other actinides, such as Th, U and Np, although no passivating role was mentioned [22]. Nevertheless, the mechanism of formation of this amorphous layer remains unknown. A local reorganisation of the hydrated and depleted fluorite structure could be considered, or a dissolution/precipitation mechanism.

The overall consistency of the kinetic rate constants (Table 4) obtained for the long-term leaching of Eq. 3 is illustrated in Fig. 9. The model A was performed with CHESS software by introducing the constants determined previously for H_2O_2 production and disproportionation and MOx oxidation. The MOx oxidation rate constant was determined from the k_U^{oxid} considering the stoichiometry $U_{0.73}Pu_{0.27}O_2$. In the model, the amorphous $Pu(OH)_4$ phase was allowed to precipitate and the uranium concentration measured after 30 days was added to the calculated ones.

Another hypothesis (model B) could be that the initial rate constant k_U^{oxid} is applicable also for the long-term dissolution, but that the disproportionation of H_2O_2 increases over time due to the Pu-enrichment of the surface. Therefore, the H_2O_2 concentration would decrease all along the experiment. As shown in Fig. 9, the long-term steady-state concentration of H_2O_2 would be around 6×10^{-9} mol.L^{-1} in order to fit the long-term concentration of uranium in solution. The corresponding disproportionation rate constant $k^{disprop}$ would be about one order of magnitude higher, as detailed in Table 4. An accurate measurement of low H_2O_2 concentrations would be necessary to discriminate among these two processes. The mechanism occurring is likely in between the two hypotheses, with both an increased disproportionation and a decreased reactivity of the surface against oxidation.

3.4.3 Homogeneous versus heterogeneous MOx radiolytic dissolution

Odorowski et al. [7] studied the radiolytic dissolution of a heterogeneous MIMAS MOx pellet with a 7 wt.% Pu content. This MIMAS fuel had plutonium-enriched agglomerates at concentrations equivalent to those of the homogeneous MOx studied here. In order to compare the behaviour of homogeneous and heterogeneous MOx, the normalized uranium mass losses were calculated according to the following equation:

$$NL(U) = \frac{m_U}{x_{solid} \times S} \quad (8)$$

with m_U the mass of dissolved uranium (g), x_{solid} the fraction of uranium in the solid and S the area of the pellets (m^2).

If the initial dissolution was very similar, the homogeneous MOx dissolution significantly decreased after one month, while the heterogeneous MOx kept dissolving at an almost constant rate (Fig. 10). The average long-term dissolution rates of the pellets are 2.8 and 25 mg.m^{-2}.d^{-1} for the homogeneous and heterogeneous MOx, respectively. The calculated dissolution rates are apparent as they did not take into account the surface evolution over time. This evolution of the surface can be significant, especially for the heterogeneous MOx for which dissolution pits can be observed (Fig 7.), and therefore the calculated NL is probably overestimated. It is interesting to note that the slope break observed for the homogeneous MOx occurs for a mass loss of about 1.7 g.m^{-2}, corresponding to an alteration thickness of about 150 nm. This thickness remains consistent with that discussed for the amorphous $Pu(OH)_4$ layer in the characterization part. The fact that the initial rates of alteration are similar for the homogeneous and heterogeneous MOx does not militate directly for a stabilization of the fluorite structure with respect to oxidation with the plutonium content. The hypothesis of the

formation of a plutonium rich layer seems to be favoured to explain the decrease of the NL(U) with time for these intense alpha radiolysis conditions.

As shown in Fig. 7, the UO_2 grains in the heterogeneous MOx were highly corroded, which explains the difference in uranium release between heterogeneous and homogeneous MOx. Considering the mechanisms observed on the homogeneous MOx with high plutonium content, these differences between UO_2 and Pu-agglomerates for the MIMAS fuel are likely due to the formation of an amorphous $Pu(OH)_4$ layer on the Pu enriched agglomerates.

The evolution of H_2O_2 concentrations was also different for both types of MOx. For the heterogeneous MIMAS MOx fuel experiment, H_2O_2 concentration linearly increased from 0 to $1.4x10^{-6}$ $mol.L^{-1}$ over one year (Fig. 11), which indicates that radiolytic production was higher than consumption. The H_2O_2 disproportionation rate was estimated to be $3.9x10^{-4}$ $mol.m^{-2}.d^{-1}$ (70% of the production), which is lower than the one measured for the present homogeneous MOx ($9.4x10^{-4}$ $mol.m^{-2}.d^{-1}$, 99% of the production). The plutonium enrichment therefore seems to have a significant effect on the consumption of hydrogen peroxide because despite a more intense alpha radiolysis and a limited oxidative dissolution, H_2O_2 in solution is not measured for the homogeneous MOx compared to the heterogeneous (Fig. 11).

Plutonium concentration quickly reached a steady state for both MOx fuels (Fig. 11), probably due to the thermodynamic equilibrium with a solid phase. The Pu concentrations are low in both cases but are slightly different: 10^{-9} M against 10^{-8} M for the homogeneous and heterogeneous MOx, respectively. As can be seen on the solubility diagrams (Fig. 5), these concentrations correspond to the solubility limits of $Pu(OH)_4(am)$ for the homogeneous MOx and the PuO_2 hydrated colloidal form for heterogeneous MOx. However, no colloids were found and, considering the uncertainty on Pu concentration in solution (80% on radiochemical measurements), Pu might be controlled by the same phase in both experiments.

4. CONCLUSION

Two successive dissolution regimes were observed during the one-year leaching of the unirradiated homogeneous $U_{0.73}Pu_{0.27}O_2$ MOx pellet in a carbonated water under argon. Released uranium was predominantly found in solution, as it forms strong soluble carbonate complexes. During the first 30 days, the release rate of uranium (tracer of the pellet dissolution) is 1.2×10^{-4} $mol.m^{-2}.d^{-1}$. The long-term uranium dissolution rate then decreases to 7.6×10^{-6} $mol.m^{-2}.d^{-1}$. The major fraction of plutonium was found on the TiO_2 reactor walls, probably sorbed. The Pu-colloidal fraction was low. The constant Pu concentration in solution (10^{-9} $mol.L^{-1}$) was consistent with a thermodynamic equilibrium in accordance with the amorphous $Pu(OH)_4$ phase. SEM – WDS analysis indicated a Pu-enriched layer at the surface of the pellets with Pu contents up to 39 wt.%, which is more resistant against leaching than the pristine surface.

The H_2O_2 concentration was under the limit of quantification LQ $1x10^{-7}$ $mol.L^{-1}$. Since the precipitation of plutonium or uranium peroxides at the surface was discarded by Raman spectroscopy, the low H_2O_2 concentration was likely due to a higher catalytic disproportionation of H_2O_2 by the Pu-enriched layer. Mass balance calculation for the long-term data showed that H_2O_2 disproportionation

represented 99 % of the H_2O_2 consumption for the homogeneous MOx, against 86 % for UO_2 pellets. The mechanism of catalytic decomposition that could involve different oxidation states of plutonium remains to be clarified.

Whatever the hypothesis, passivation or enhanced disproportionation, the plutonium enrichment explains the two dissolution regimes observed on the homogeneous MOx with high plutonium content. It can also explain the different behaviours observed for heterogeneous MIMAS MOx between UO_2 grains and plutonium enriched zones.

These results are of clear interest for the behaviour of any type of MOx fuel in storage pools or under environmental and radioactive waste repository conditions, among others to support the reactive transport modelling used in performance assessment [37], as well as for the understanding of the mixed plutonium/uranium oxide chemistry.

ACKNOWLEDGMENT

This study was carried out under the COSTO research program funded jointly by the CEA, ANDRA and EDF. The authors are grateful to the personnel of the Atalante facility for their technical support and specifically C. Marques and N. Vaissières for the solution analyses, J. Delrieu for the annealing of the pellets and the Raman spectroscopy and J.R Sevilla for the SEM-WDS analyses. The authors also greatly acknowledge the relevant and detailed comments of two anonymous reviewers that helped to improve the accuracy and quality of the paper. The research leading to these results has received funding from the European Commission Horizon 2020 Research and Training Programme of the European Atomic Energy Community (EURATOM) (H2020-NFRP-2016-2017-1) under grant agreement n° 755443 (DisCo project).

REFERENCES

[1] M. Odorowski, C. Jégou, L. De Windt, V. Broudic, G. Jouan, S. Peuget, C. Martin, Effect of metallic iron on the oxidative dissolution of UO_2 doped with a radioactive alpha emitter in synthetic Callovian-Oxfordian groundwater, Geochim. Cosmochim. Acta. 219 (2017) 1–21. doi:10.1016/j.gca.2017.08.043.

[2] D.W. Shoesmith, Fuel corrosion processes under waste disposal conditions, J. Nucl. Mater. (2000). doi:10.1016/S0022-3115(00)00392-5.

[3] C. Poinssot, C. Ferry, P. Lovera, C. Jégou, J.M. Gras, Spent fuel radionuclide source term model for assessing spent fuel performance in geological disposal. Part II: Matrix alteration model and global performance, J. Nucl. Mater. 346 (2005) 66–77. doi:10.1016/j.jnucmat.2005.05.021.

[4] J. De Pablo, F. Clarens, F. El Aamrani, M. Rovira, The Effect of Hydrogen Peroxide Concentration on the Oxidative Dissolution of Unirradiated Uranium Dioxide, Mat. Res. Soc. Symp. Proc. 663 (2001) 409–416.

[5] S. Stroes-Gascoyne, F. Garisto, J.S. Betteridge, The effects of alpha-radiolysis on UO_2 dissolution determined from batch experiments with Pu-doped UO_2, J. Nucl. Mater. (2005). doi:10.1016/j.jnucmat.2005.04.069.

[6] I. Casas, J. De Pablo, F. Clarens, J. Giménez, J. Merino, J. Bruno, A. Martínez-Esparza, Combined effect of H_2O_2 and HCO^{3-} on UO_2(s) dissolution rates under anoxic conditions, Radiochim. Acta. 97 (2009) 485–490. doi:10.1524/ract.2009.1641.

[7] M. Odorowski, C. Jégou, L. De Windt, V. Broudic, S. Peuget, M. Magnin, M. Tribet, C. Martin, Oxidative dissolution of unirradiated Mimas MOx fuel (U/Pu oxides) in carbonated water under oxic and anoxic conditions, J. Nucl. Mater. 468 (2016) 17–25. doi:10.1016/j.jnucmat.2015.09.059.

[8] C. Jégou, R. Caraballo, J. De Bonfils, V. Broudic, S. Peuget, T. Vercouter, D. Roudil, Oxidizing dissolution of spent MOX47 fuel subjected to water radiolysis: Solution chemistry and surface characterization by Raman spectroscopy, J. Nucl. Mater. 399 (2010) 68–80. doi:10.1016/j.jnucmat.2010.01.004.

[9] C. Jégou, R. Caraballo, S. Peuget, D. Roudil, L. Desgranges, M. Magnin, Raman spectroscopy characterization of actinide oxides $(U_{1-y}Pu_y)O_2$: Resistance to oxidation by the laser beam and examination of defects, J. Nucl. Mater. 405 (2010) 235–243. doi:10.1016/j.jnucmat.2010.08.005.

[10] L. Bauhn, N. Hansson, C. Ekberg, P. Fors, R. Delville, K. Spahiu, The interaction of molecular hydrogen with α-radiolytic oxidants on a $(U,Pu)O_2$ surface, J. Nucl. Mater. 505 (2018) 54–61. doi:10.1016/j.jnucmat.2018.04.006.

[11] Eurachem, CITAC, EURACHEM/CITAC Guide CG 4; Quantifying uncertainty in analytical measurement, Third Edition, (2012).

[12] S. Sunder, Calculation of radiation dose rates in a water layer in contact with used CANDU UO_2 fuel, Nucl. Technol. 122 (1997) 211–221. doi:10.13182/NT98-A2863.

[13] D. Serrano-Purroy, I. Casas, E. González-Robles, J.P. Glatz, D.H. Wegen, F. Clarens, J.

Giménez, J. De Pablo, A. Martínez-Esparza, Dynamic leaching studies of 48 MWd/kgU UO_2 commercial spent nuclear fuel under oxic conditions, J. Nucl. Mater. 434 (2013) 451–460. doi:10.1016/j.jnucmat.2011.03.020.

[14] C. Jégou, M. Gennisson, S. Peuget, L. Desgranges, G. Guimbretière, M. Magnin, Z. Talip, P. Simon, Raman micro-spectroscopy of UOX and MOx spent nuclear fuel characterization and oxidation resistance of the high burn-up structure, J. Nucl. Mater. 458 (2015) 343–349. doi:10.1016/j.jnucmat.2014.12.072.

[15] V. V. Rondinella, T. Wiss, The high burn-up structure in nuclear fuel, Mater. Today. 13 (2010) 24–32. doi:10.1016/S1369-7021(10)70221-2.

[16] G. Jouan, M. Virot, E. Buravand, SEM analyzes of powdered actinide compounds : Implementation in a hot laboratory, in: HOTLAB, 2016.

[17] J. van der Lee, L. De Windt, V. Lagneau, P. Goblet, Module-oriented modeling of reactive transport with HYTEC, Comput. Geosci. 29 (2003) 265–275. doi:10.1016/S0098-3004(03)00004-9.

[18] E. Giffaut, M. Grivé, P. Blanc, P. Vieillard, E. Colàs, H. Gailhanou, S. Gaboreau, N. Marty, B. Madé, L. Duro, Andra thermodynamic database for performance assessment: ThermoChimie, Appl. Geochemistry. 49 (2014) 225–236. doi:10.1016/j.apgeochem.2014.05.007.

[19] J.M. Elorrieta, D. Manara, L.J. Bonales, J.F.F. Vigier, O. Dieste, M. Naji, R.C. Belin, V.G. Baonza, R.J.M.J.M. Konings, J. Cobos, Raman study of the oxidation in (U, Pu)O_2 as a function of Pu content, J. Nucl. Mater. 495 (2017) 484–491. doi:10.1016/j.jnucmat.2017.08.043.

[20] B. Muzeau, C. Jégou, F. Delaunay, V. Broudic, A. Brevet, H. Catalette, E. Simoni, C. Corbel, Radiolytic oxidation of UO_2 pellets doped with alpha-emitters ($^{238/239}$Pu), J. Alloys Compd. 467 (2009) 578–589. doi:10.1016/j.jallcom.2007.12.054.

[21] R.J. Lemire, F. Garisto, The solubility of U, Np, Pu, Th and Tc in a geological disposal vault for used nuclear fuel, At. Energy Canada Limited, AECL. (1989).

[22] V. Neck, J.I. Kim, Solubility and hydrolysis of tetravalent actinides, Radiochim. Acta. 89 (2001) 1–16. doi:10.1524/ract.2001.89.1.001.

[23] L.E. Sweet, J.F. Corbey, F. Gendron, J. Autschbach, B.K. McNamara, K.L. Ziegelgruber, L.M. Arrigo, S.M. Peper, J.M. Schwantes, Structure and bonding investigation of plutonium peroxocarbonate complexes using cerium surrogates and electronic structure modeling, Inorg. Chem. 56 (2017) 791–801. doi:10.1021/acs.inorgchem.6b02235.

[24] M. Amme, B. Renker, B. Schmid, M.P. Feth, H. Bertagnolli, W. Döbelin, Raman microspectrometric identification of corrosion products formed on UO_2 nuclear fuel during leaching experiments, J. Nucl. Mater. 306 (2002) 202–212. doi:10.1016/S0022-3115(02)01291-6.

[25] S. Bastians, G. Crump, W.P. Griffith, R. Withnall, Raspite and studtite: Raman spectra of two unique minerals, J. Raman Spectrosc. 35 (2004) 726–731. doi:10.1002/jrs.1176.

[26] J. Rothe, C. Walther, M.A. Denecke, T. Fanghänel, XAFS and LIBD investigation of the formation and structure of colloidal Pu(IV) hydrolysis products, Inorg. Chem. 43 (2004) 4708–4718. doi:10.1021/ic049861p.

[27] O.A. Maslova, G. Guimbretière, M.R. Ammar, L. Desgranges, C. Jégou, A. Canizarès, P. Simon, Raman imaging and principal component analysis-based data processing on uranium oxide ceramics, Mater. Charact. 129 (2017) 260–269. doi:10.1016/j.matchar.2017.05.015.

[28] E. Ekeroth, O. Roth, M. Jonsson, The relative impact of radiolysis products in radiation induced oxidative dissolution of UO_2, J. Nucl. Mater. (2006). doi:10.1016/j.jnucmat.2006.04.001.

[29] C.M. Lousada, M. Trummer, M. Jonsson, Reactivity of H_2O_2 towards different UO_2-based materials: The relative impact of radiolysis products revisited, J. Nucl. Mater. (2013). doi:10.1016/j.jnucmat.2011.06.003.

[30] A. Hiroki, J.A. LaVerne, Decomposition of hydrogen peroxide at water-ceramic oxide interfaces, J. Phys. Chem. B. 109 (2005) 3364–3370. doi:10.1021/jp046405d.

[31] R. Pehrman, M. Trummer, C.M. Lousada, M. Jonsson, On the redox reactivity of doped UO_2 pellets – Influence of dopants on the H_2O_2 decomposition mechanism, J. Nucl. Mater. 430 (2012) 6–11. doi:10.1016/j.jnucmat.2012.06.016.

[32] S. Nilsson, M. Jonsson, H_2O_2 and radiation induced dissolution of UO_2 and SIMFUEL pellets, J. Nucl. Mater. 410 (2011) 89–93. doi:10.1016/j.jnucmat.2011.01.020.

[33] P.A. Korzhavyi, L. Vitos, D.A. Andersson, B. Johansson, Oxidation of plutonium dioxide, Nat. Mater. 3 (2004) 225–228. doi:10.1038/nmat1095.

[34] S. Sunder, N.H. Miller, D.W. Shoesmith, Corrosion of uranium dioxide in hydrogen peroxide solutions, Corros. Sci. (2004). doi:10.1016/j.corsci.2003.09.005.

[35] P.G. Keech, J.J. Nö El, D.W. Shoesmith, The electrochemical reduction of hydrogen peroxide on uranium dioxide under intermediate pH to acidic conditions, Electrochim. Acta. 53 (2008) 5675–5683. doi:10.1016/j.electacta.2008.03.008.

[36] C. Maillard, J.M. Adnet, Plutonium(IV) peroxide formation in nitric medium and kinetics Pu(VI) reduction by hydrogen peroxide, Radiochim. Acta. 89 (2001) 485–490. doi:10.1524/ract.2001.89.8.485.

[37] L. De Windt, N.F. Spycher, Reactive Transport Modeling: A Key Performance Assessment Tool for the Geologic Disposal of Nuclear Waste, Elements. 15 (2019) 99–102. doi:10.2138/gselements.15.2.99.

LIST OF FIGURES

Fig. 1. EPMA analysis of the sample (2x130 steps of 35 µm). Weight percentages are consistent with stoichiometry $(U_{0.73}Pu_{0.27})O_2$ and do not vary beyond 10%.

Fig. 2. Uranium concentration during the pre-leaching steps of the homogeneous MOx in carbonated water ($[NaHCO_3] = 10^{-3}$ mol.L^{-1}) under anoxic atmosphere (argon atmosphere, $[O_2] < 2$ vppm)

Fig. 3. Total aqueous concentration of uranium and plutonium during the leaching of the homogeneous MOx pellets in carbonated water ($[NaHCO_3] = 10^{-2}$ mol.L^{-1}) under anoxic conditions (argon atmosphere, $[O_2] < 2$ vppm).

Fig. 4. Distribution of uranium and plutonium between the solution, the colloids, and the sorbed/precipitated fraction on the TiO_2 reactor at the end of the leaching experiments in carbonated water ($[NaHCO_3] = 10^{-2}$ mol.L^{-1}) under anoxic conditions (argon atmosphere, $[O_2] < 2$ vppm).

Fig. 5. Solubility diagrams of uranium and plutonium as a function of redox potential (V/SHE). The diagrams were plotted at a temperature of 25 °C, a pH of 9, an activity of HCO_3^- of 10^{-2}. The red dots represent the experimental concentrations for the homogeneous MOx (this work), and the blue squares the heterogeneous MOx [7].

Fig. 6. SEM images of the homogeneous MOx after one year of leaching in carbonated water ($[NaHCO_3] = 10^{-2}$ mol.L^{-1}) under anoxic conditions (argon atmosphere, $[O_2] < 2$ vppm); the occurrence of corrosion pits is scarce (right).

Fig. 7. (left) SEM image of a heterogeneous MIMAS MOx fuel after one year of leaching in carbonated water ($[NaHCO_3] = 10^{-2}$ mol.L^{-1}) under anoxic conditions (argon atmosphere, $[O_2] < 2$ vppm); the occurrence of corrosion pits is high and corresponds to the UO_2-enriched zones (right, SEM-WDS analysis, U in green, Pu in orange) [7].

Fig. 8. Typical Raman spectra of the homogeneous MOx pellet before and after leaching in carbonated water ($[NaHCO_3] = 10^{-2}$ mol.L^{-1}) under anoxic conditions (argon atmosphere, $[O_2] < 2$ vppm).

Fig. 9. Modelling of the long-term kinetic leaching of the homogeneous MOx pellet in carbonated water ($[NaHCO_3] = 10^{-2}$ mol.L^{-1}) under anoxic conditions (argon atmosphere, $[O_2] < 2$ vppm). The model A considers the long-term rate constant of the MOx oxidation, the model B considers the initial rate constant of the MOx oxidation (with an enhanced long-term rate constant of disproportionation).

Fig. 10. Comparison of the evolution of the uranium normalized mass loss during the leaching of homogeneous (this work) and heterogeneous MOx [7] in carbonated water ($[NaHCO_3] = 10^{-2}$ mol.L^{-1}) under anoxic conditions (argon atmosphere, $[O_2] < 2$ vppm).

Fig. 11. Comparison of the evolution of H_2O_2 and plutonium concentrations in solution during the leaching of homogeneous (this work) and heterogeneous MOx [7] in carbonated water ($[NaHCO_3] = 10^{-2}$ mol.L^{-1}) under anoxic conditions (argon atmosphere, $[O_2] < 2$ vppm).

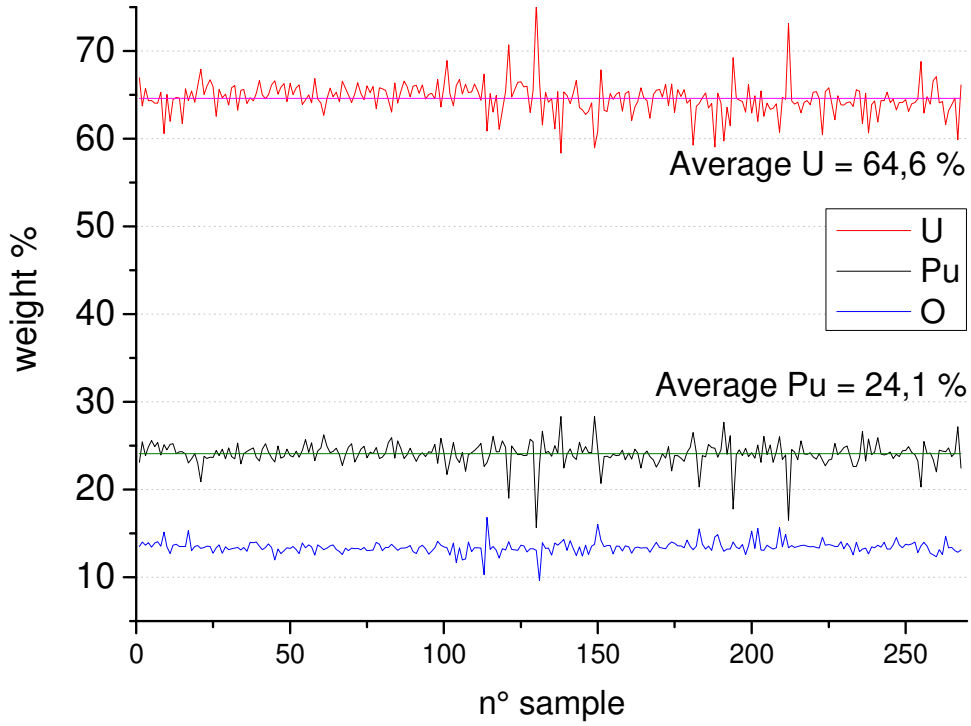

Fig. 2. EPMA analysis of the sample (2x130 steps of 35 µm). Weight percentages are consistent with stoichiometry $(U_{0.73}Pu_{0.27})O_2$ and do not vary beyond 10%.

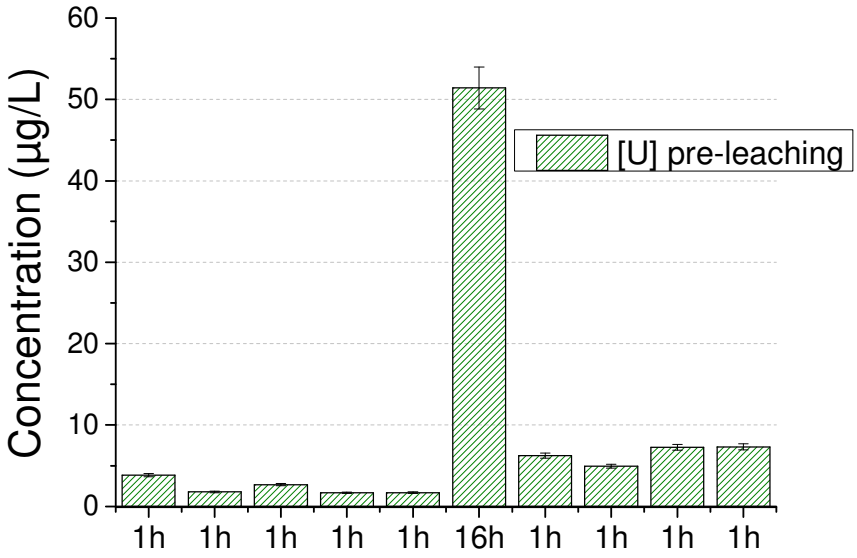

Fig. 2. Uranium concentration during the pre-leaching steps of the homogeneous MOx in carbonated water ($[NaHCO_3] = 10^{-3}$ mol.L^{-1}) under anoxic atmosphere (argon atmosphere, $[O_2] < 2$ vppm).

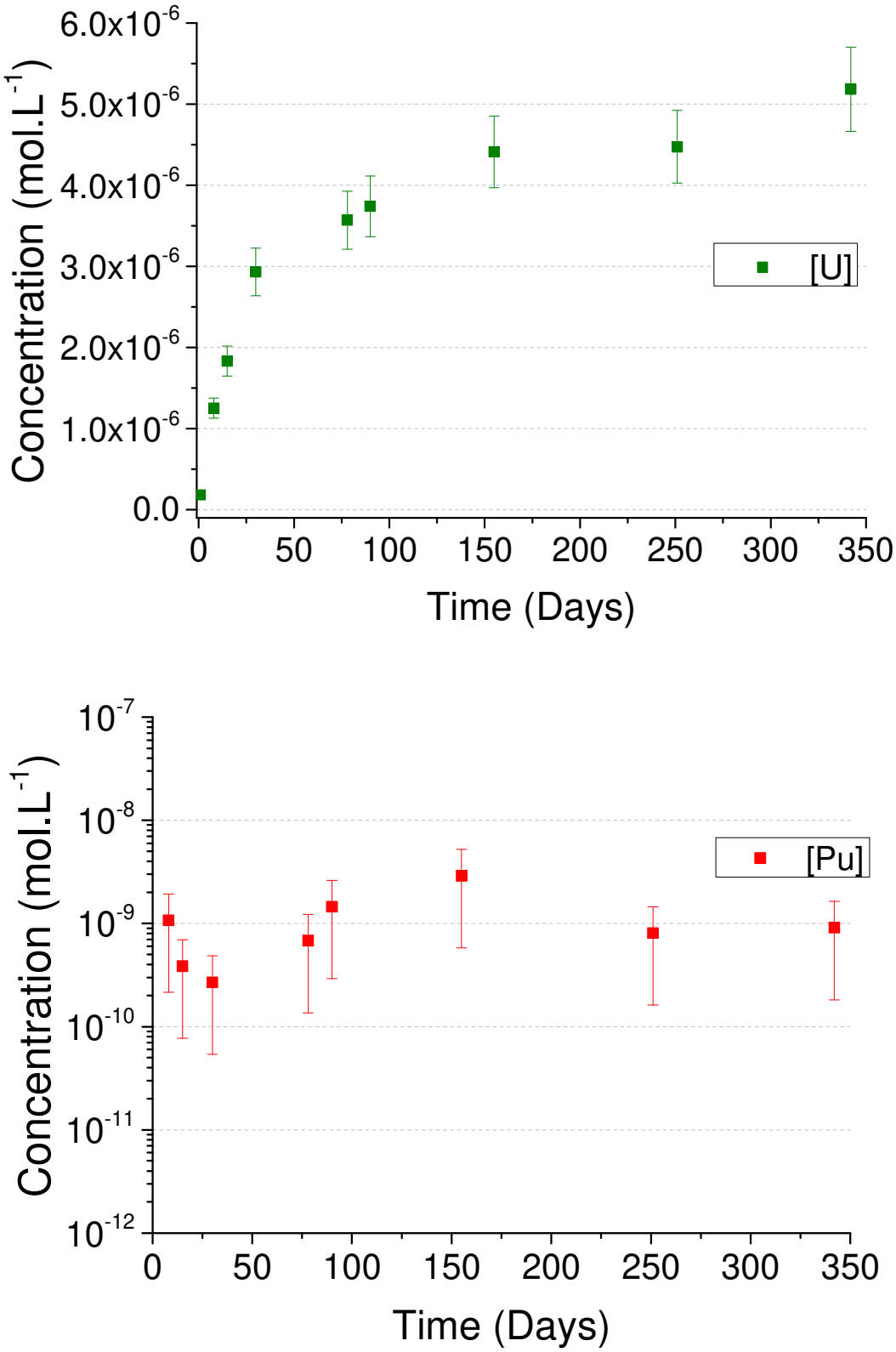

Fig. 3. Total aqueous concentration of uranium and plutonium during the leaching of the homogeneous MOx pellets in carbonated water ($[NaHCO_3] = 10^{-2}$ mol.L^{-1}) under anoxic conditions (argon atmosphere, $[O_2] < 2$ vppm).

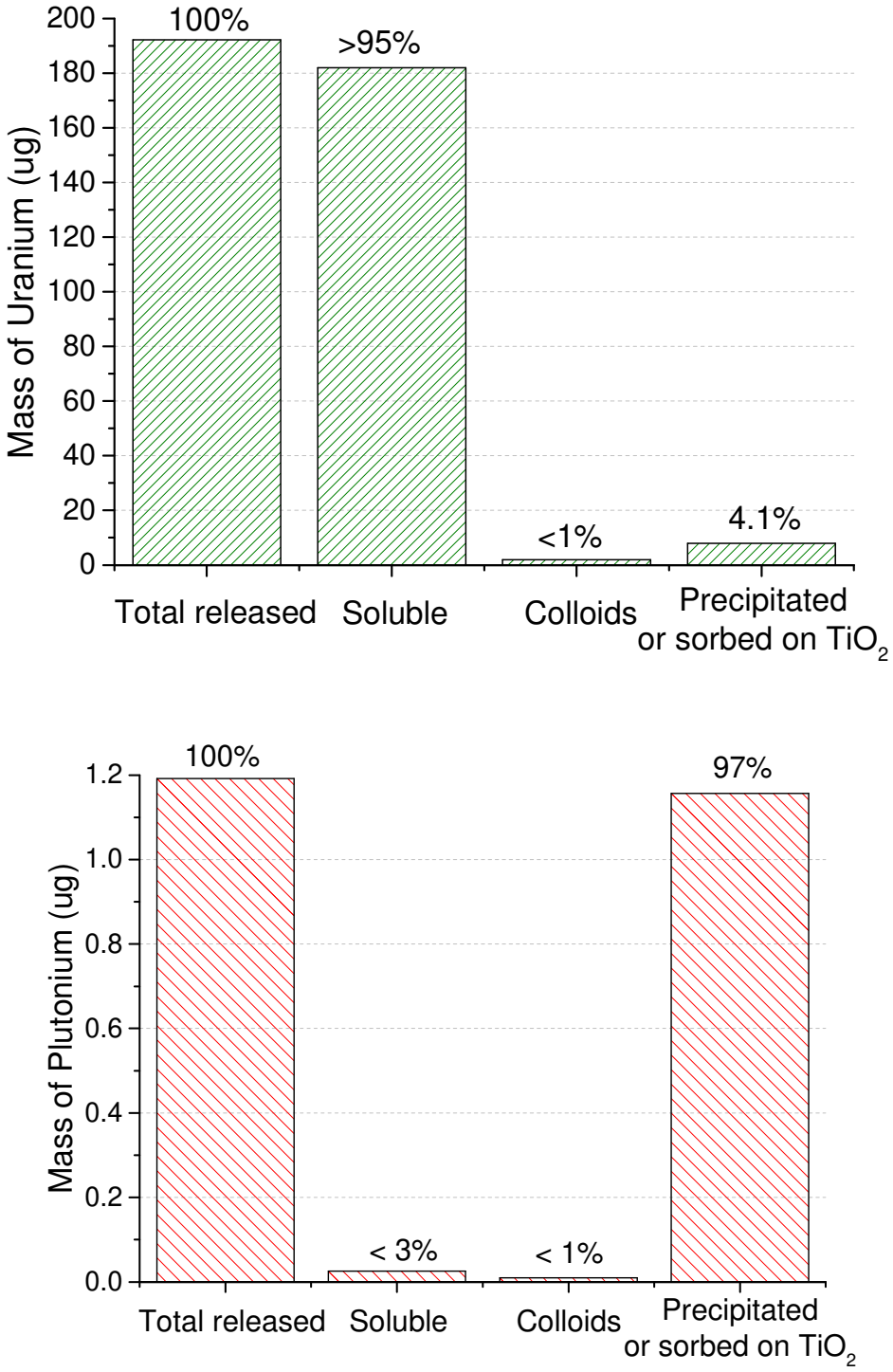

Fig. 4. Distribution of uranium and plutonium between the solution, the colloids, and the precipitated (and sorbed) fraction on the TiO_2 reactor at the end of the leaching experiments in carbonated water ($[NaHCO_3] = 10^{-2}$ mol.L^{-1}) under anoxic conditions (argon atmosphere, $[O_2] < 2$ vppm).

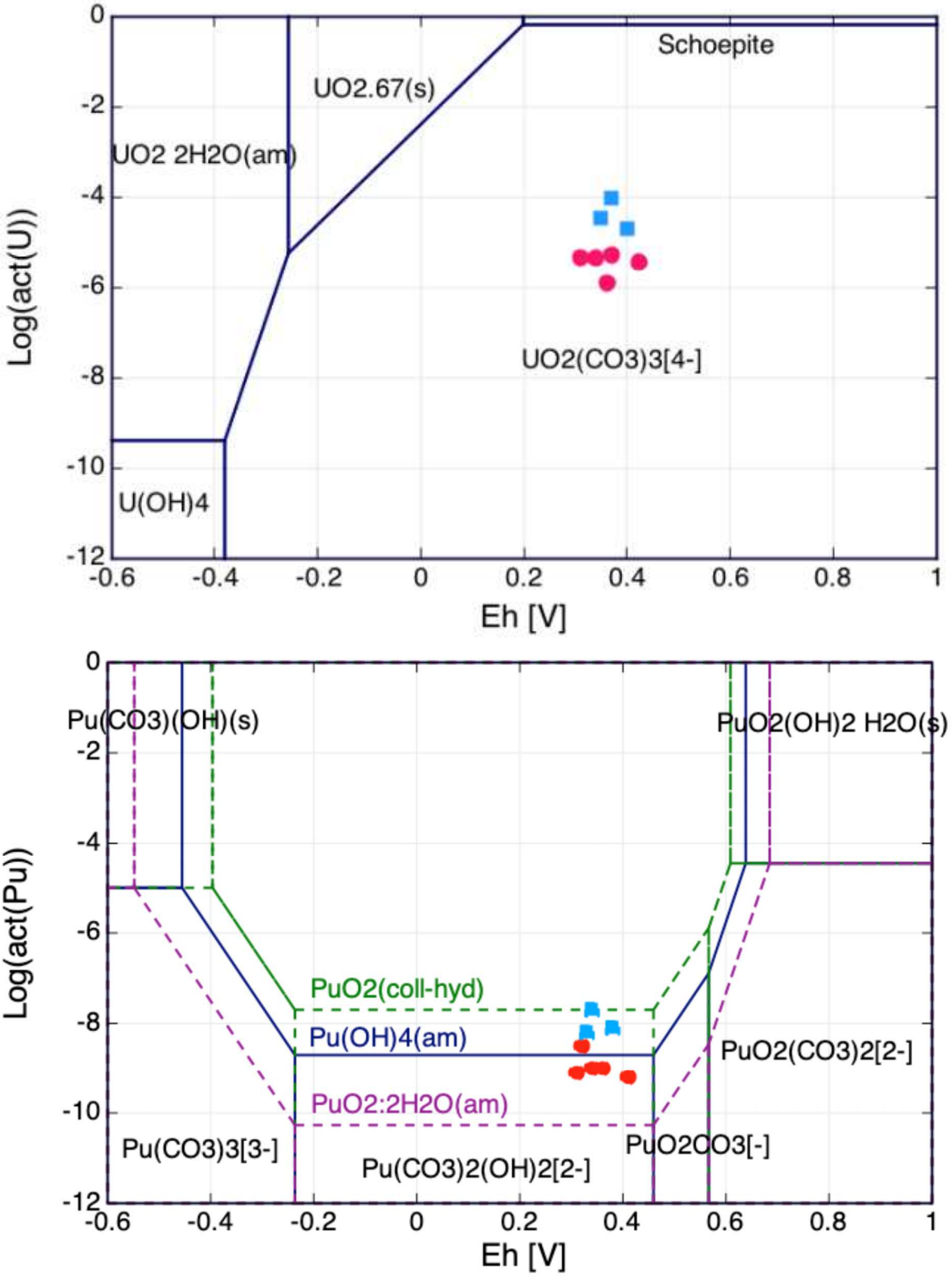

Fig. 5. Solubility diagrams of uranium and plutonium as a function of redox potential (V/SHE). The diagrams were plotted at a temperature of 25 °C, a pH of 9, an activity of HCO_3^- of 10^{-2}. The red dots represent the experimental concentrations for the homogeneous MOx (this work), and the blue squares the heterogeneous MOx [7].

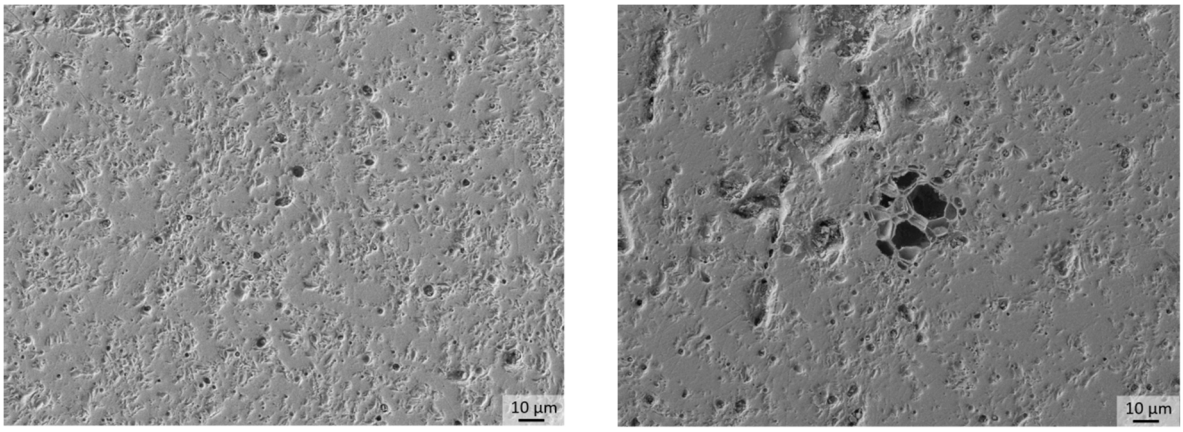

Fig. 6. SEM images of the homogeneous MOx after one year of leaching in carbonated water ([$NaHCO_3$] = 10^{-2} mol.L^{-1}) under anoxic conditions (argon atmosphere, [O_2] < 2 vppm); the occurrence of corrosion pits is scarce (right).

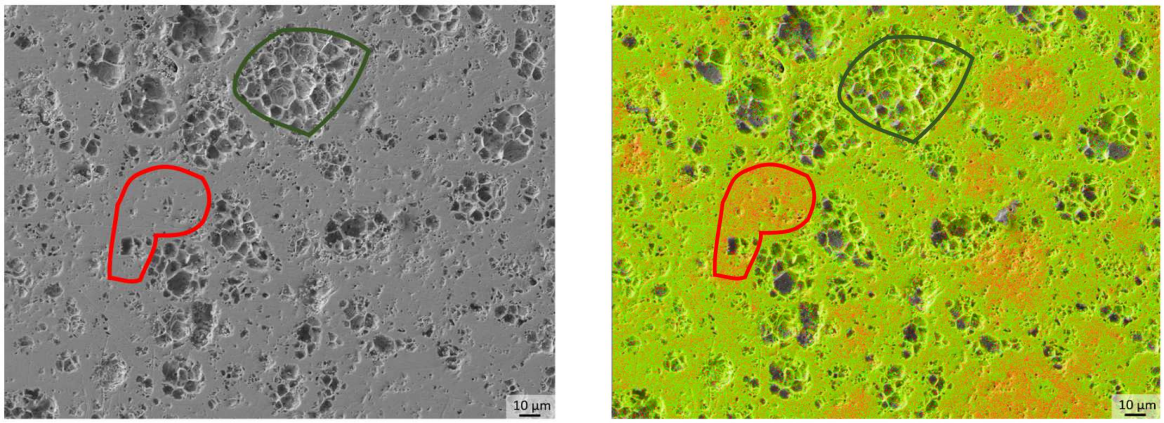

Fig. 7. (left) SEM image of a heterogeneous MIMAS MOx fuel after one year of leaching in carbonated water ([$NaHCO_3$] = 10^{-2} mol.L^{-1}) under anoxic conditions (argon atmosphere, [O_2] < 2 vppm); the occurrence of corrosion pits is high and corresponds to the UO_2-enriched zones (right, SEM-WDS analysis, U in green, Pu in orange) [7].

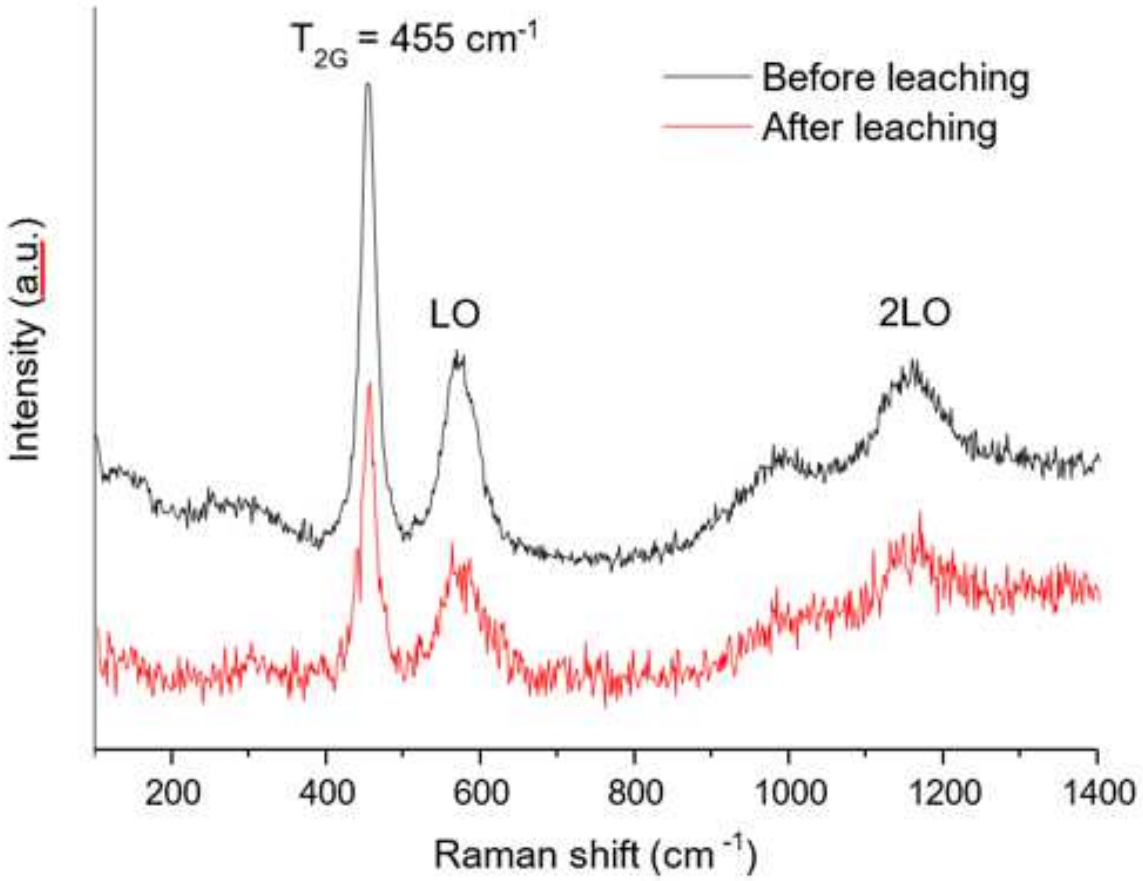

Fig. 8. Typical Raman spectra of the homogeneous MOx pellet before and after leaching in carbonated water ($[NaHCO_3] = 10^{-2}$ mol.L^{-1}) under anoxic conditions (argon atmosphere, $[O_2] < 2$ vppm).

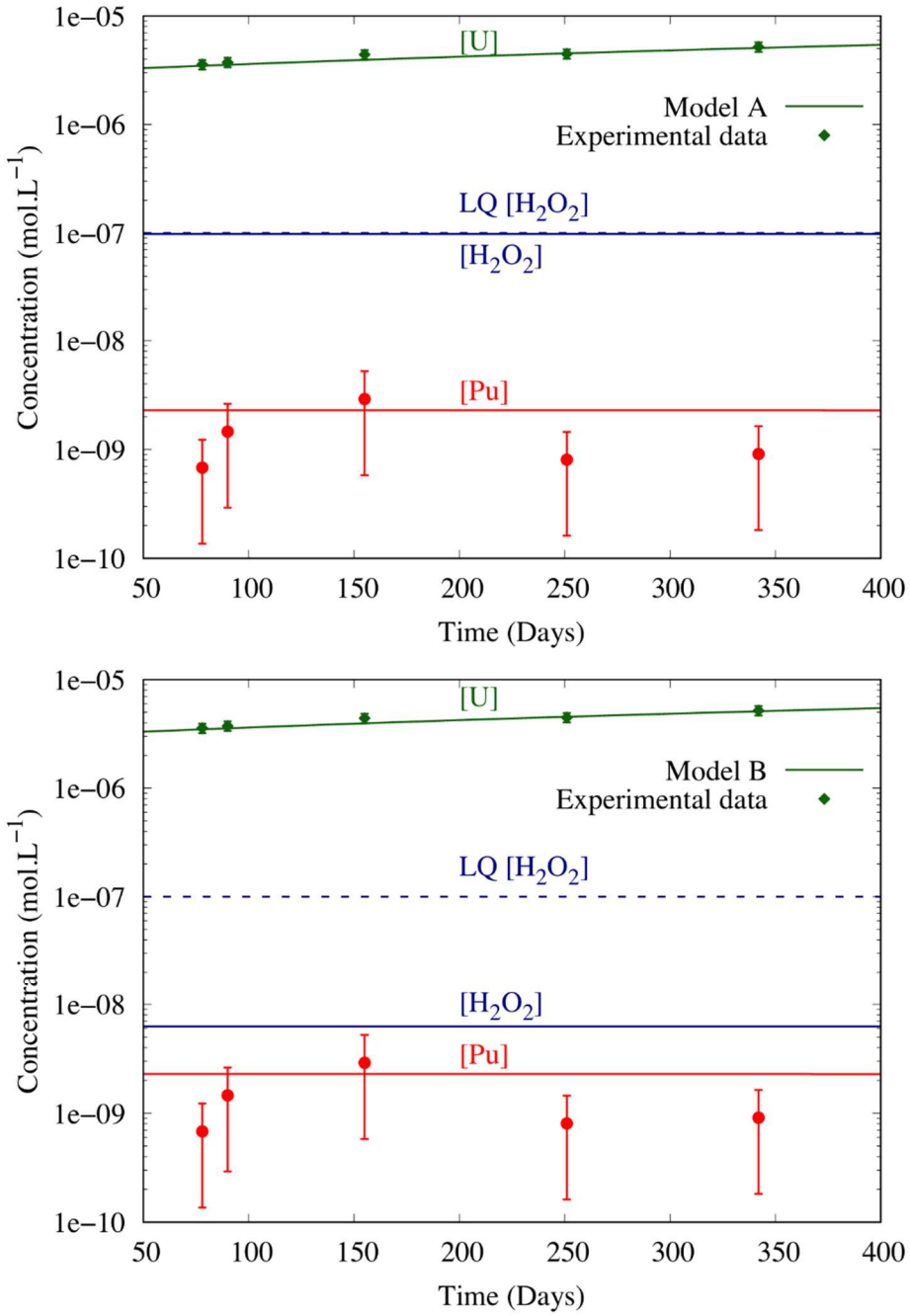

Fig. 9. Modelling of the long-term kinetic leaching of the homogeneous MOx pellet in carbonated water ([$NaHCO_3$] = 10^{-2} mol.L^{-1}) under anoxic conditions (argon atmosphere, [O_2] < 2 vppm). The model A considers the long-term rate constant of the MOx oxidation, the model B considers the initial rate constant of the MOx oxidation (with an enhanced long-term rate constant of disproportionation).

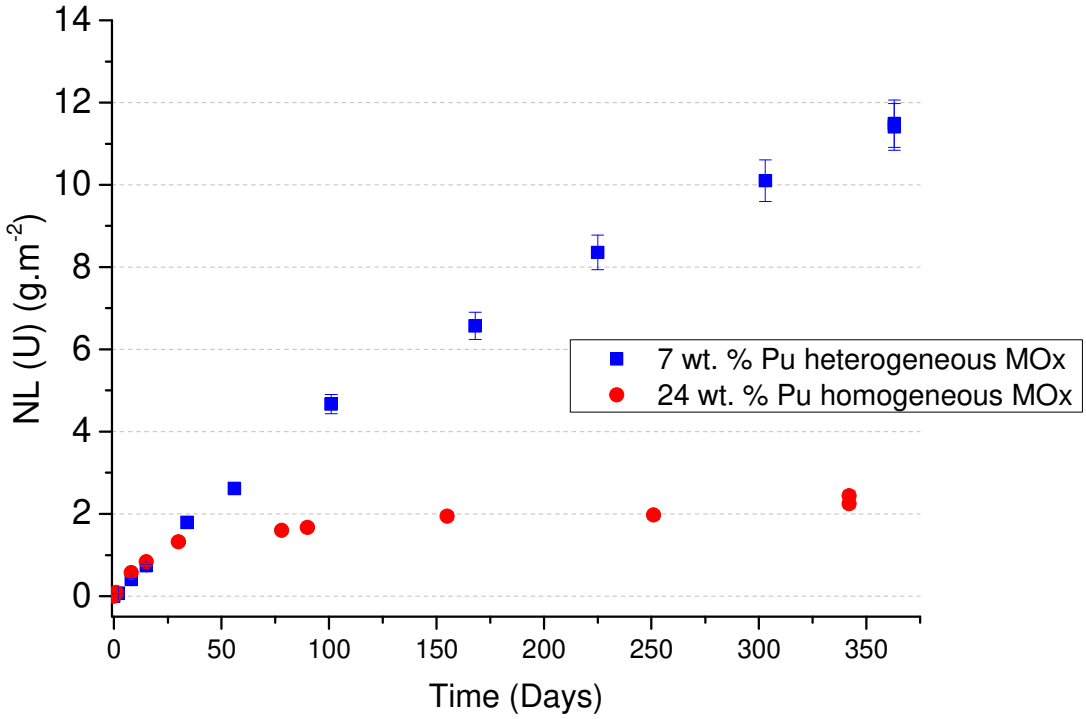

Fig. 10. Comparison of the evolution of the uranium normalized mass loss during the leaching of homogeneous (this work) and heterogeneous MOx [7] in carbonated water ([$NaHCO_3$] = 10^{-2} mol.L^{-1}) under anoxic conditions (argon atmosphere, [O_2] < 2 vppm).

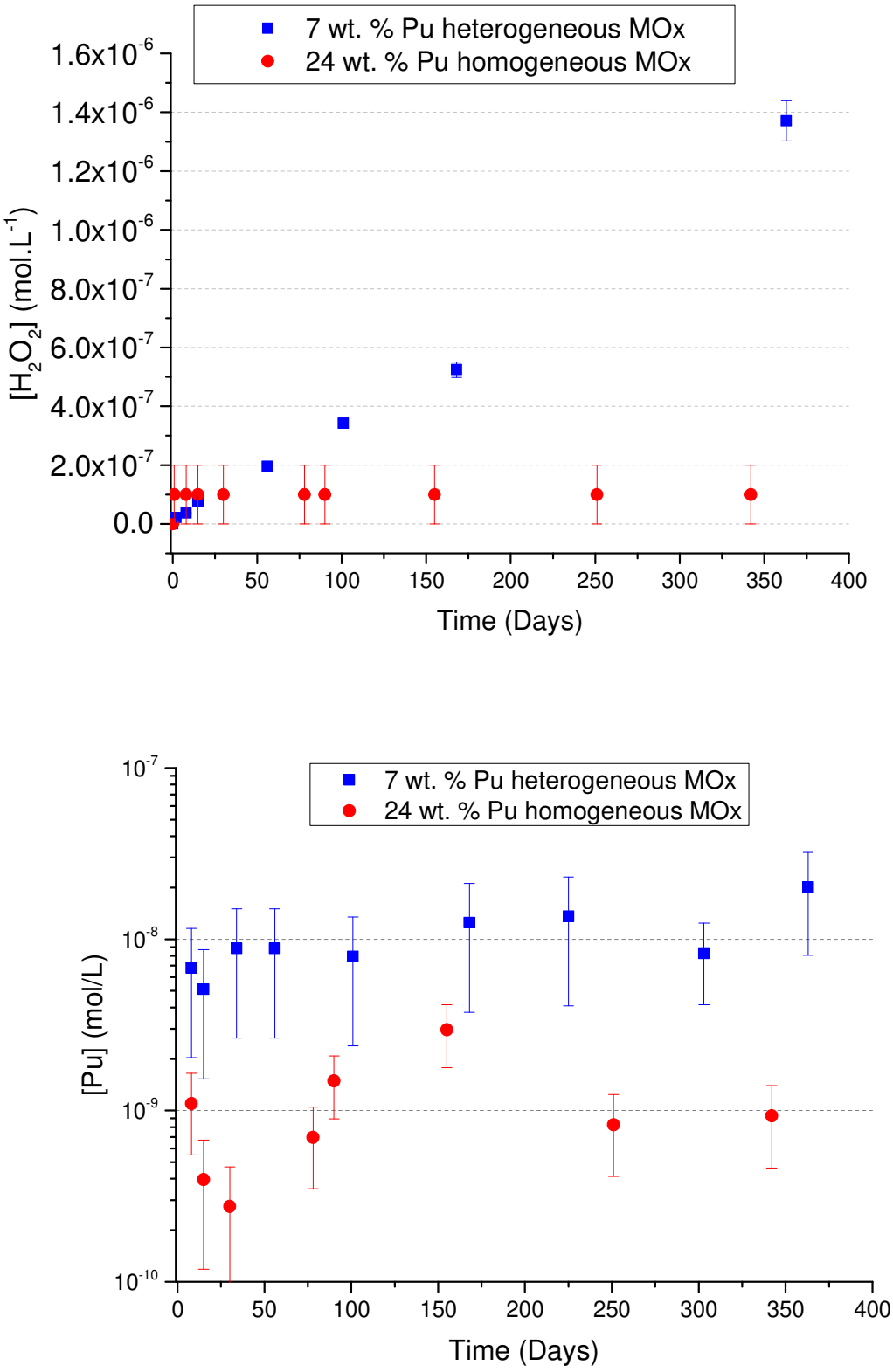

Fig. 11. Comparison of the evolution of H_2O_2 and plutonium concentrations in solution during the leaching of homogeneous (this work) and heterogeneous MOx [7] in carbonated water ($[NaHCO_3] = 10^{-2}$ mol.L^{-1}) under anoxic conditions (argon atmosphere, $[O_2] < 2$ vppm).

LIST OF TABLES

Table 1. Characteristics of the two MOx pellets used in the experiments (expanded uncertainties with a coverage factor k=2 [11]).

Table 2. Chemical and isotopic compositions of the homogeneous MOx after isotopic decay calculations (0.1% uncertainties considered).

Table 3. Uranium and plutonium wt.% at the surface of the pellet after leaching in carbonated water determined by SEM-WDS analysis.

Table 4. Kinetic rate constants used in the long-term geochemical model (Eq. 3, Fig. 9).

Table 1.

Characteristics of the two MOx pellets used in the experiments (expanded uncertainties with a coverage factor k=2 [11]).

Pellets	Diameter (mm)	Height (mm)	Weight (g)	Specific Surface $x10^{-4}$ (m^2/g)
1	5.400 ± 0.010	0.93 ± 0.05	0.2129 ± 0.0005	2.871 ± 0.035
2	5.400 ± 0.010	0.96 ± 0.05	0.2227 ± 0.0005	

Table 2.

Chemical and isotopic compositions of the homogeneous MOx after isotopic decay calculations (0.1% uncertainties considered).

U/(U+Pu) (wt.%)	Pu/(U+Pu) (wt.%)	X/U_{tot} (wt.%)		X/Pu_{tot} (wt.%)					
		^{235}U	^{238}U	^{238}Pu	^{239}Pu	^{240}Pu	^{241}Pu	^{242}Pu	^{241}Am
73.02	26.98	0.75	99.25	0.17	69.98	24.42	0.88	1.08	3.47

Table 3.

Uranium and plutonium wt.% at the surface of the pellet after leaching in carbonated water determined by SEM-WDS analysis.

57 spectra	U/(U+Pu) (wt.%)	Pu/(U+Pu) (wt.%)
Average	60.7	39.3
Min	55.0	34.8
Max	65.2	45.0
Standard deviation	2.2	2.2

Table 4.

Kinetic rate constants used in the geochemical model (Eq. 3, Fig. 9).

	Model A	Model B
k^{prod} (mol.m^2.s^{-1})	1.1×10^{-8}	
k^{oxid}_U (L.m^{-2}.s^{-1})	8.8×10^{-4}	1.4×10^{-2}
k^{oxid}_{MOx} (L.m^{-2}.s^{-1})	1.2×10^{-3}	1.9×10^{-2}
$k^{disprop}$ (L.m^{-2}.s^{-1})	1.1×10^{-1}	17×10^{-1}